RESEARCH LETTER

Shallow seismic reflection imaging of the Inabanga–Clarin portion of the North Bohol Fault, Central Visayas, Philippines

Romer Carlo T. Gacusan[1,2*] and Alfredo Mahar Francisco A. Lagmay[1,2]

Abstract

On 15 October 2013, a magnitude 7.2 earthquake was generated from a previously unidentified fault in the island of Bohol. This fault was named the North Bohol Fault (NBF) by authorities. We investigated the geometry of the Inabanga–Clarin portion of the NBF using three high-resolution shallow seismic reflection profiles to image sections of the fault up to 150 m depth not seen in trenching and regional offshore seismic profiles. These seismic profiles are along the Calubian, Napo, and Caluwasan transects which run perpendicular to the N40°E strike of the NBF. Reverse faults were identified in the Calubian and Napo profiles, whereas a positive flower structure was seen in the Caluwasan profile. Normal faults were also identified in the Caluwasan and Napo profiles. This study corroborates the observations in earlier trenching studies that measured the reverse fault dip angle and direction of the NBF at 70° SE. It also demonstrates that topographic flexures are the surface manifestation of steeply dipping faults. The downthrown block of the reverse faults in the Calubian profile defines a depression on the surface; the Napo seismic profile displacement of 3 m is consistent with the 3-m-high surface rupture in Barangay Anonang; and the flower structure in the Caluwasan profile is related to the pressure ridge and right lateral offset stream on the surface. Furthermore, the presence of normal faults as well as the other deformational features is consistent with the transpressional regime described in the literature, wherein the principal horizontal stress is oriented NW–SE. These findings complement earlier geomorphic and trenching investigations of the NBF and demonstrate the application of a tool to image the subsurface and characterize undescribed or hidden faults, which is necessary for earthquake hazard assessment and attendant risk mitigation and prevention planning.

Keywords: Shallow seismic reflection, Bohol earthquake, Seismic hazard assessment, Subsurface deformation, Transpression

Background

The Negros–Cebu–Bohol region is one of the areas with the highest occurrence of strong (> M5.0) earthquakes in the Philippines in the past 30 years (Fig. 1A). Earthquake occurrences in the region were possibly caused by the active compression accommodating the slip of the left-lateral Philippine Fault (Aurelio 2000; Yoshida et al. 2016). Identification of unmapped faults in the region has been a challenge since fault-related structures are weakly expressed and concealed on the surface due to erosion coupled by thick vegetation in a humid tropical environment. This is the case of the M_w 7.2 Bohol earthquake on 15 October 2013, which occurred along the previously unmapped North Bohol Fault (NBF). The 2013 Bohol event is the strongest recorded earthquake in the region to date, leading to 222 deaths and damage amounting to US$52.06 million (NDRRMC 2013; PHIVOLCS 2013; Lagmay and Eco 2014). The lack of understanding on the previously unidentified fault failed to prepare the communities against earthquake hazards during the 2013 Bohol temblor. Assessment of seismic hazards require accurate knowledge of fault parameters including location, geometry, slip rate, recurrence interval, and recent

*Correspondence: gacusan115@gmail.com
[1] National Institute of Geological Sciences, University of the Philippines, Quezon City, Philippines
Full list of author information is available at the end of the article
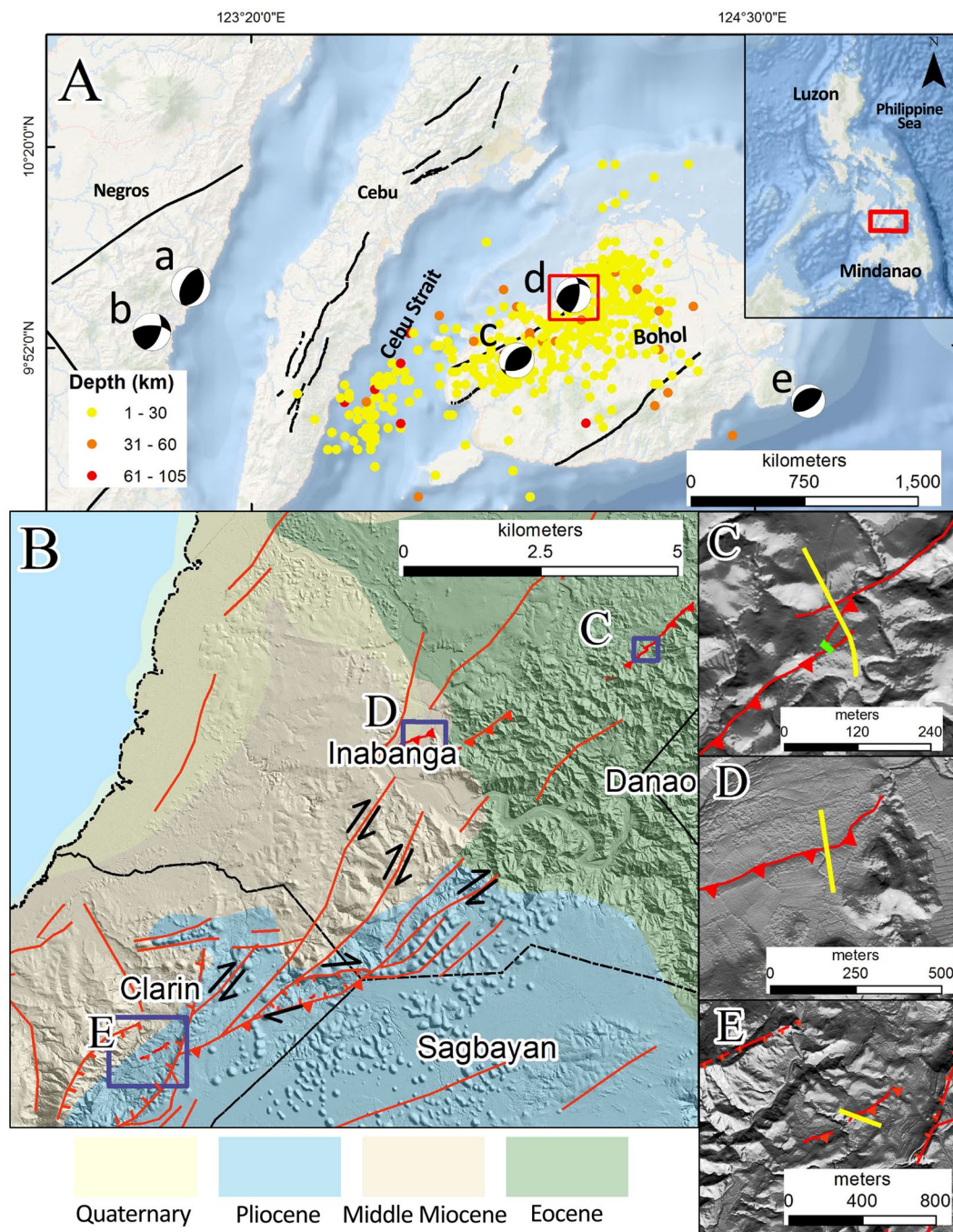
Fig. 1 **A** Aftershocks recorded 4 months after 15 October 2013 Temblor. The focal mechanisms of instrumentally recorded significant earthquakes in the region are also shown (a—2012 M6.7; b—2012 M6.0; 2013 M7.2; d—1996 M5.2; e—1990 M6.6); black lines represent the location of active faults in the region identified by PHIVOLCS. **B** Geological map of the Inabanga–Clarin segment of the North Bohol Fault showing the location of the 2013 earthquake ground rupture (red lines). Discussion of geology is described in text. The blue boxes enclose the location of the Calubian, Napo, and Caluwasan seismic transects laid over the post-earthquake LiDAR image as shown in **C**–**E**, respectively. Green line in **C** represents the location of the trench of Rimando (2015). Sources of data: focal mechanism of a, b, d, and e: USGS; aftershocks and focal mechanism of c: PHIVOLCS; geologic map from BMG (1987); location of 2013 ground rupture from Felix (2017); LiDAR: UP DREAM Program

kinematics, which are obtained through surface geologic mapping, paleoseismic trenching, and geodetic surveys. Subsurface data are also necessary to further construe its geometry, kinematics, and dynamics, which are not always evident on the surface.

The centroid moment tensor (CMT) solution recorded by Philippine Institute of Volcanology and Seismology (PHIVOLCS) indicates a reverse fault earthquake with minor right-lateral displacement (Fig. 1A). The magnitude 7.2 caused by the 2013 Temblor corresponds to about 3-m maximum fault displacement and 60- to 100-km-long rupture length (Wells and Coppersmith 1994). This is evident from the surface rupture in Barangay Anonang in the municipality of Inabanga, Bohol, and the 90- to 100-km-long distribution of earthquake epicenters that extends nearly up to the southern part of Cebu (Fig. 1A). A regional seismic reflection profile confirms the extent of the NBF trace offshore in the Cebu Strait and also shows the SE dipping thrust behavior of the NBF, which formed a NE-trending anticline composed of reefal limestones (Aurelio et al. 2013). Such fault–fold relationship is also expressed on land in Maribojoc–Loon Peninsula where a NE-striking anticline affected Pliocene limestones that formed the Chocolate Hills (Aurelio et al. 2013; Rimando 2015). Paleoseismic trenching showed that the NBF steepens its dip up to 70°SE as it propagates down to depth. Dating of organic materials obtained from the trench revealed at least two earthquakes occurred along the NBF in the past 12 ka (Rimando 2015). On the surface, morphotectonic analysis using pre- and post-earthquake high-resolution digital terrain models (DTMs) revealed both left and right lateral strike slip features along the strike of the NBF (Felix 2017). The contrasting morphotectonic features along the strike of the NBF were attributed to the kinematic reorganization of the Philippine Sea Plate during the Pliocene, where its movement changes from north to northwest with respect to the Eurasian Plate (Aurelio 2000).

One key aspect of fault characterization not addressed in previous studies is the determination of the geometry of the NBF at depths up to 150 m. Fault geometry at these depths is often more complex compared to the geometry at seismogenic depths because of the increase in pressure and temperature, which suppresses brittle branching of faults (Ben-Zion and Sammis 2003; Haberland et al. 2007). Such complexity in thrust faults are expressed as gaps because surface rupture is not always manifested (Stein and King 1984; Stein and Yeats 1989), and folding associated with fault bends (Suppe 1983) and propagating thrust faults (Suppe and Medwedeff 1990). Although regional-scale seismic data sets are often used to constrain the overall geometry and kinematics of fault, these data sets fail to describe the fault from the near-surface

up to 500 m depth because the seismic resolution of the regional-scale data is often traded for coverage extent. Furthermore, the seismic data used for interpreting the subsurface geometry of the NBF were gathered prior to the 2013 earthquake, thus the emergent post-earthquake geometry of the fault was not clearly described. Consequently, a data gap commonly exists between the surface geologic data and deeper regional-scale images of faults (Dolan and Pratt 1997; Pratt et al. 2002; Bruno et al. 2011). This gap may impede the accurate characterization of the NBF's shallow geometry since fault branches are also subject to future fault movement.

The data gap between surface or near-surface geology and deeper faults can be supplemented by high-resolution shallow seismic reflection data to better constrain the nature of faulting. In this study, we investigated the Inabanga–Clarin portion of the NBF, where the fault is best exposed and described. The seismic profiles were correlated with earlier geomorphic and trenching studies to form an integrated analysis of the North Bohol Fault.

Study area

Three sites along the Inabanga–Clarin portion of the North Bohol Fault were chosen based on the location of ground deformation sites as seen through post-earthquake Light Detection and Ranging (LiDAR)-derived images. The first site located in Sitio Calubian in the municipality of Inabanga is a knickzone between hilly and flat terrain and characterized by three left-stepping faults oriented N40–60°E (Fig. 1C). Ground rupture morphology in the area varies from hanging wall collapse to simple thrust to pressure ridges, which are attributed to the thickness of soil cover and, to some extent, the degree of weathering of the andesites in the locality (Fig. 1B; Felix 2017). The stepover exhibits scarp height variation from northwest to southeast measured as 1 m, 0.9 m, and 1.5 m, respectively. The Calubian trench located 40 m southwest of the seismic transect also revealed highly weathered andesite flows associated with the Eocene Ubay Formation, which consists mainly of at least 250-m-thick volcanic deposits (Rimando 2015). The subsurface trace of the 0.9- and 1.5-m-high scarps was observed in the trench as high-angle faults dipping 55°SE and 70°SE, respectively (Rimando 2015).

The second site located in Barangay (village) Napo in Inabanga is a flat plain adjacent to the Inabanga River (Fig. 1D). The NBF trace reappears in a floodplain as a 0.03- to 0.25-m-high fault scarp oriented N75°E dipping 64°NW (Felix 2017). Sand boils associated with the 2013 earthquake were also observed in the southwestern tip of the fault trace immediately before it terminates near the river (Felix 2017). The area is overlain by 400- to 800-m-thick Middle Miocene sedimentary rocks of the

Carmen Formation, which unconformably overlies the Eocene unit (Peña 2008). This formation consists of mudstone, sandstone, and shale (Corby et al. 1951; Mula and Maac 1995). Siltstones were also observed in nearby outcrops and in the Luwak trench (Rimando 2015) located 1.2 km southeast of the profile.

The third site is located within a large pull-apart structure in Barangay Caluwasan in the municipality of Clarin (Fig. 1E). In this area, the ground rupture trace is expressed as 2-m-high pressure ridges along a gently sloping terrain. The fault continues to the southwest showing right-stepping features after crossing a right-lateral offset stream (Felix 2017). The northwestern boundary of the pull-apart structure exhibits beds dipping 5–30°SE, whereas the southeastern boundary show beds dipping at 5°NW (BMG 1987). The lithology of the area is mostly covered by a 1.5-km-thick Pliocene sequence composed of conglomerate, limestone, and marl, which belongs to the Maribojoc Formation (BMG 1987; Rimando 2015). This formation unconformably overlies the Middle Miocene sediments (Peña 2008).

Shallow seismic reflection

The shallow seismic reflection surveys used in this study were acquired 14 months after the 2013 Bohol earthquake. Parameters used for acquiring raw seismic data were similar for all three data sets. A 48-channel Geometrics Geode seismic acquisition system with a 14 lb. sledgehammer source was used to image the fault up to 100 m depth. Receiver stations were spaced at 5-m intervals using 100 Hz geophones. Shots collocated with the receivers were stacked with three shots and recorded for 1.5 ms with a 0.250 ms sampling rate.

Data were analyzed using Reflexw software and followed the conventional common midpoint (CMP) processing sequence of shallow seismic data sets (Baker 1999; Yilmaz 1987). Geometry information of the raw seismic records were extracted from the trace headers of each file and rechecked with field notes. A scaling function was then applied to balance the amplitude of the signals and to normalize the effects of wavefront divergence and damping (Sandmeier 2016).

Interactive velocity adaptations were done to differentiate the velocity of the reflection events from coherent noise (i.e., refractions, air waves, and ground roll) and to estimate the depth of the shallowest reflecting layer. Reflection events in the shot gathers were further distinguished since they exhibited the classical hyperbolic move-out behavior and were clearly visible over different bands of test frequency filters.

Elevation and refraction static corrections were used to correct the static time shifts on each seismic trace caused by topographic variability and lateral thickness variation of the weathering layer, respectively. For the elevation statics, shot and receiver elevations were derived from the LiDAR DTM, wherein the lowest elevation along the seismic transect was set as datum (Baker 1999). In addition, replacement velocities, which range from 1000 to 1500 m/s, were obtained from the velocity adaptations of the direct arriving energy. Refraction statics, on the other hand, were first obtained using an inversion algorithm that calculates a two-layered velocity model that satisfies the manually picked travel times of the first arriving seismic energy. The static time corrections are then derived for each trace based on this model.

Pre-stack processing which includes trace edit, deconvolution, bandpass filter, and muting were applied to minimize ambient and coherent noise in the data and to improve signal-to-noise ratio (S/N) (Fig. 2). Trace edit was applied to suppress the noisy traces. Spiking deconvolution with a 6 ms filter length obtained from the autocorrelation function of the optimum reflection window was used to enhance the reflection signals. A 0.1 percent pre-whitening was also introduced before deconvolving the data to ensure numerical stability (Yilmaz 1987; Mousa and Al-Shuhail 2011). An Ormsby bandpass frequency filter was designed with sloping cut-off frequencies to avoid the ringy character of the signals called Gibbs phenomenon. Although the bandpass filter removed high-frequency noise, coherent noise still remained in the data. The remaining coherent noise was removed through muting the refractions and noise cone data (Baker et al. 1998; Baker 1999).

Each trace was then rearranged according to their assigned CMPs for dynamic corrections, namely velocity analysis, normal move-out (NMO) correction, residual statics, and stacking. Velocity analysis was performed using constant velocity stacks (CVS) and unnormalized crosscorrelation of CMP gathers. CVS panels were obtained at 100 m/s intervals over 800–2500 m/s range, whereas unnormalized crosscorrelation was calculated from 500 to 3500 m/s at 50 m/s intervals. The CVS panels and velocity hyperbolas which produced the most coherent reflection signals were used to generate the interval velocity model for NMO correction. The NMO and residual statics-corrected gathers were then stacked and depth-converted to generate the final seismic profiles.

For the Calubian data set, spectral whitening was used instead of spiking deconvolution because the data in this transect exhibited low S/N ratios. In addition, an f–k filter was also applied to eliminate velocities 1000 m/s, thus removing noise that includes the residual components of surface waves, which are more prevalent in this data set.

Gacusan and Lagmay *Geosci. Lett.*   (2019) 6:9

Page 5 of 10
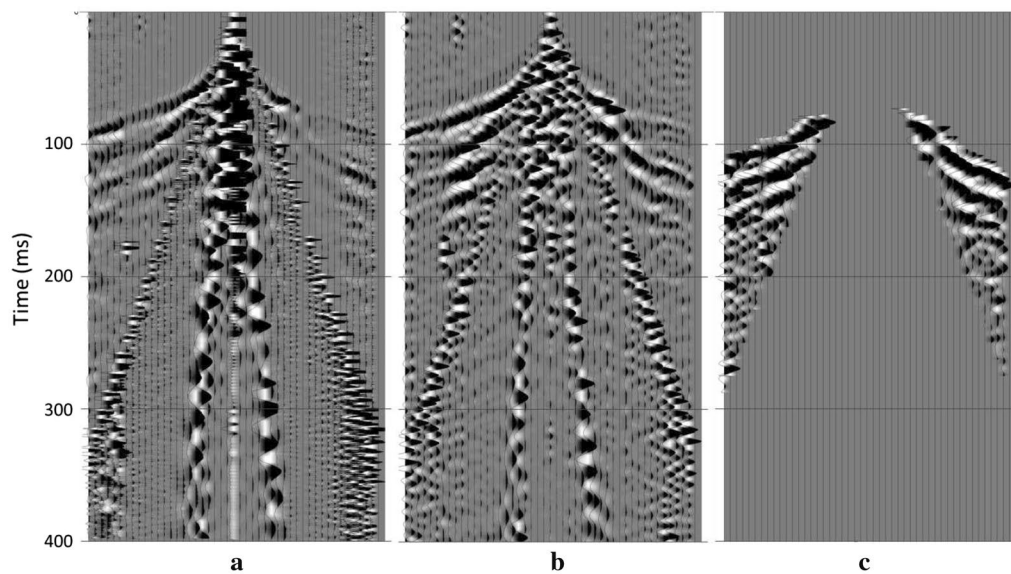
Fig. 2 Representative field file of Napo data showing the improvement of reflections during processing. **a** Shot gather with applied scaled window gain, trace edits, and static corrections. **b** The application of spiking deconvolution and bandpass filter improved the quality of reflections. **c** Muting of unwanted signals (i.e., refractions, air waves, and ground roll) further improved clarity of the reflections

Results and discussion

The high-resolution seismic reflection profiles showed SE dipping faults located at depths of up to 120 m. These structures are likely the subsurface extent of the North Bohol Fault since their surface projection coincides with the location of the coseismic scarps of the 2013 event. There are also newly identified faults that are expressed as linear geomorphic features on the surface. In general, inferred fault traces in all seismic profiles are distinguished by offsets, cutoffs, abrupt change of signal behavior, and disruption of coherent signals.

Calubian profile

The Calubian seismic profile is presented with the profile of the morphology, the location of faults as seen in a paleoseismic trench of Rimando (2015), and the interpretation of seismic reflection signals (Fig. 3). There are two faults that are interpreted based on the truncation of reflection signals. The first structure is a 70°NW dipping reverse fault which is identified from 38–100 m depth. This structure coincides with a surface rupture and a break in slope. The second fault dips 72°SE and is identified from 35 to 115 m depth. This fault corresponds to the fault which appears in the paleoseismic trench. In between these two reverse faults is the footwall block downthrown relative to the hanging wall blocks on either side and define a low-lying portion in the surface morphology. Based on the geologic cross

section of Rimando (2015), the Calubian profile represents the Eocene deposits of the Ubay Formation.
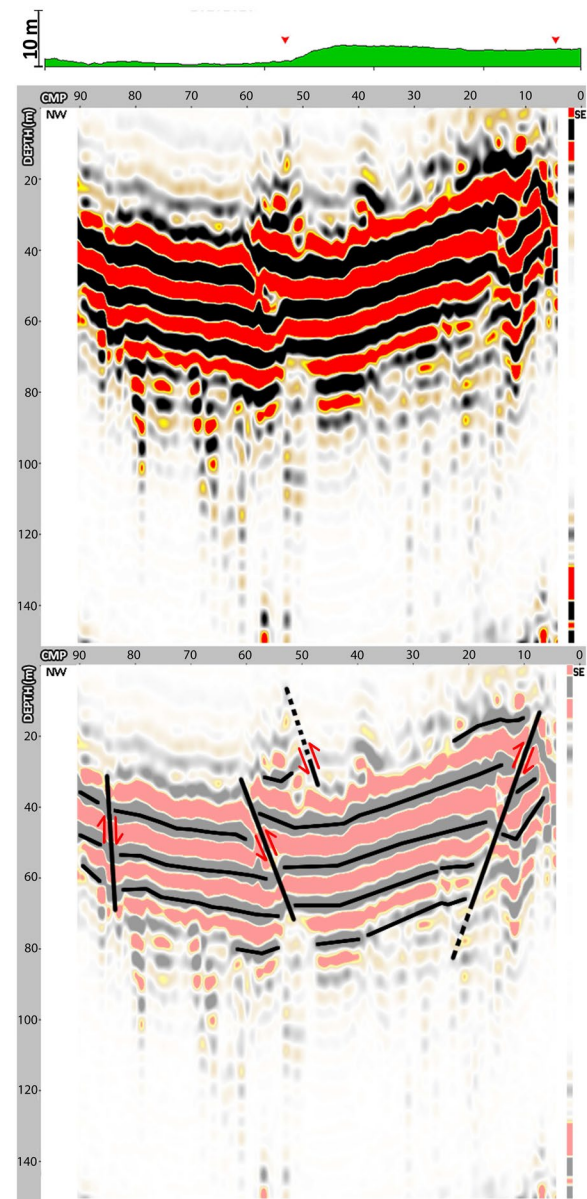
Napo profile

The Napo seismic profile is described with the topographic cross section and the location of the faults as seen on the surface (Fig. 4). There are four discontinuities interpreted as faults based on the offset and disruption of coherent reflection signals. From left to right: (1) a normal fault dipping 79°SE, which is identified from 38 to 65 m depth and cuts siltstones by 2 m. There are no geomorphic features that can be used to correlate with this structure; (2) the surface manifestation of the fault scarp when projected downward to 38 m depth coincides with reflection signals that are truncated. We interpret this truncation as evidence that the 70°SE dipping reverse fault extends downward up to 38 m depth. This is the same method of interpretation in the example given by Dolan and Pratt (1997) and Pratt et al. (1998) for the Santa Monica Fault. The cross section of the scarp and this fault resembles a fold formed by a propagating reverse slip as described in Suppe and Medwedeff (1990) (Fig. 5); (3) a 63°SE dipping reverse fault is identified from 38–80 m. This fault cuts siltstones by 3 m, which is consistent with the height of the fault scarp exposed in Barangay Anonang. The zone between CMP 51 and 63 is defined as a contractional relay (Nicol et al. 2002) attributed to the contact between the siltstones and the younger deposits (Fig. 4). This structure is formed when

Gacusan and Lagmay *Geosci. Lett.* (2019) 6:9
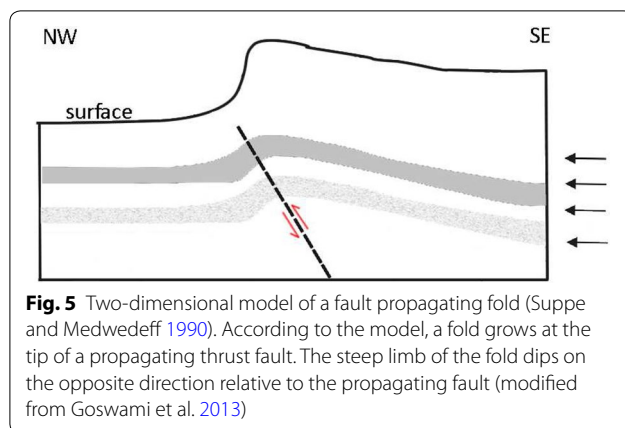
Page 6 of 10
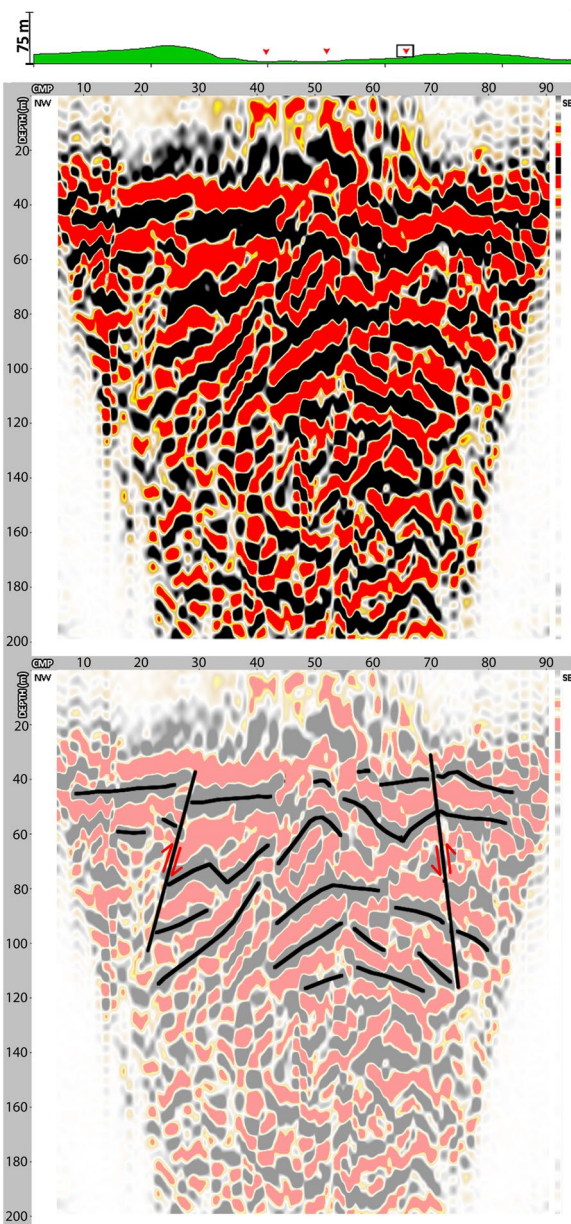
Fig. 3 (top) Topographic cross section and (bottom) interpreted CDP stacked section of the Calubian seismic line showing that the location of the NBF trace in the trench (red box). Red arrows represent the location of the ruptures on the surface. Vertical exaggeration for the topographic cross section is ×2, while the seismic profile has no vertical exaggeration
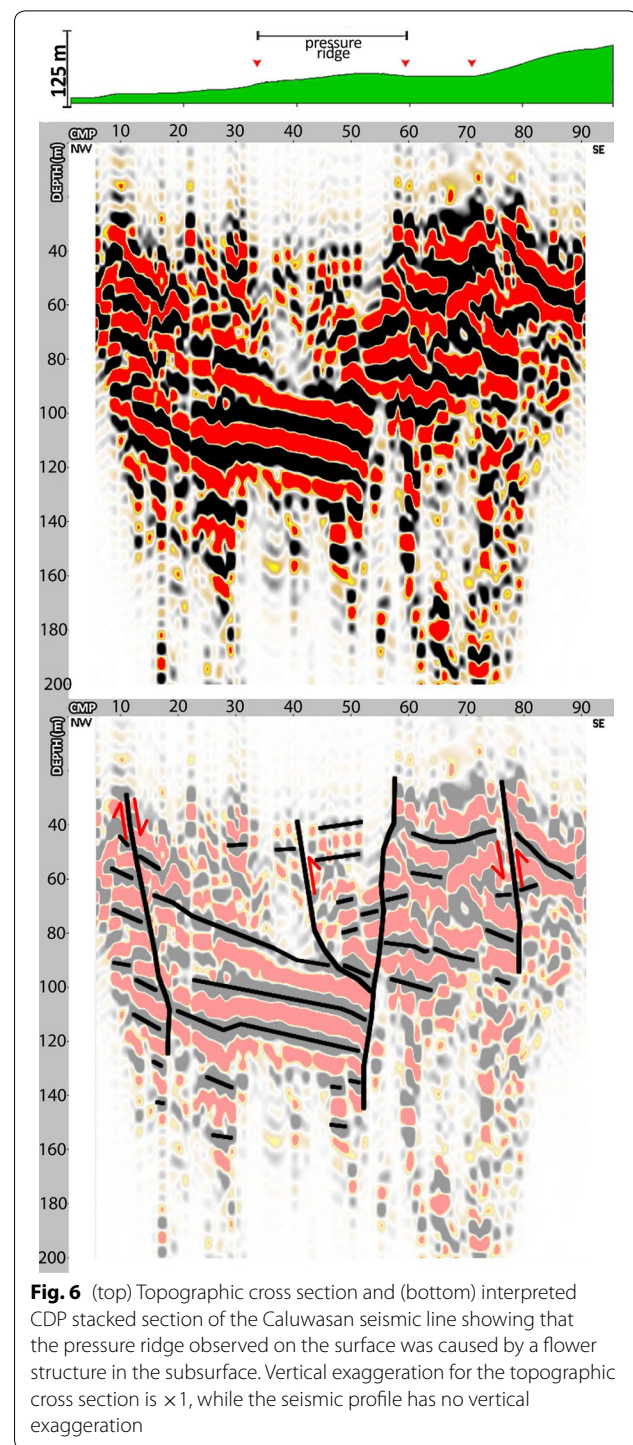
Fig. 4 (top) Topographic cross section and (bottom) interpreted CDP stacked section of the Napo seismic line showing that the NBF exhibits vertical segmentation attributed to a lithologic contact between the Middle Miocene sediments and the younger alluvial deposits. Vertical exaggeration for the topographic cross section is ×5, while the seismic profile has no vertical exaggeration

the lateral propagation of the North Bohol Fault bifurcates due to mechanical heterogeneity (Nicol et al. 2002); (4) a reverse fault that dips 67°NW and truncates the siltstones from 15 to 60 m depth. This structure corresponds to a northeast-trending linear feature that terminates before converging with the main fault trace. The range of velocities in the profile ranges from 900 to 1100 m/s, which are associated with the siltstones observed by Rimando (2015) in the Luwak trench. The reflection-free region above the siltstones in the seismic profile (< 35 m depths) is associated with loose deposits of the Inabanga River, which caused sand boils observed southwest of the profile.

Fig. 5 Two-dimensional model of a fault propagating fold (Suppe and Medwedeff 1990). According to the model, a fold grows at the tip of a propagating thrust fault. The steep limb of the fold dips on the opposite direction relative to the propagating fault (modified from Goswami et al. 2013)

Caluwasan profile

The Caluwasan seismic profile is presented with the profile of the morphology and the location of surface ruptures as seen on the surface (Fig. 6). Four structures were identified in the profile based on discontinuities of the reflection signals. From left to right: (1) a normal fault dipping 74°SE and is identified between 35 and 100 depth. This structure displaces the reflection signals by approximately 5 m. There are no geomorphic features that can be used to correlate this fault. The structure, however, could be due to the localized extension within the pull-apart structure (Fig. 1B, E); (2) a reverse fault that dips 77°SE and cuts the weak reflections from 40 to 100 m depth. This fault coincides with the simple pressure ridge on the surface; (3) an 81°NW dipping reverse fault is identified at 25–140 depth. This structure corresponds to a scarp as seen in the topographic profile. Faults 2 and 3 in the profile are connected and are found in the zone between CMP 39 and 58. This zone where two reverse faults converge at 100 m depth defines a flower structure. The flower structure accommodates a component of lateral motion and is associated with a bulge as seen in the cross-sectional profile. At this part on the surface, there is also a right lateral offset stream, but is not seen in the profile; (4) a reverse fault that dips 74°SE and cuts the reflection events from 30 to 100 m depth. This structure also coincides with a scarp on the surface. Reflection signals at 40 m depth dip to the southwest, which is interpreted as drag folds related to fault movement. Based on geologic the cross sections of BMG (1987) and Rimando (2015), the upper 150 m of the Caluwasan profile represents the Pliocene deposits of the Maribojoc Formation. The reflection-free region above the 30 m is possibly associated with the clays and limestone cavities as described in the radargrams of MGB (2014), located 200 m northeast of

Fig. 6 (top) Topographic cross section and (bottom) interpreted CDP stacked section of the Caluwasan seismic line showing that the pressure ridge observed on the surface was caused by a flower structure in the subsurface. Vertical exaggeration for the topographic cross section is ×1, while the seismic profile has no vertical exaggeration

the Caluwasan profile. Reflection signals at 85–100 m depth range dip gently southeastwards at 12° were possibly the deeper expression of the 5–30°SE dipping beds in the area (BMG 1987). Termination of these horizons suggest that deposition of this unit is fault controlled and the dipping beds is caused by fault drag.

Gacusan and Lagmay *Geosci. Lett.*   (2019) 6:9

Page 8 of 10

Implications

The seismic profiles showed complex shallow subsurface structures of the North Bohol Fault in the Inabanga–Clarin portion and characterized by a variety of deformational features. In Sitio Calubian, the NBF trace is associated with a surface depression; in Napo, the NBF exhibited a contractional relay associated with a simple scarp on the surface; in Caluwasan, the fault trace showed a positive flower structure related to the pressure ridge on the surface. The orientation of these structures suggests that the principal stress is directed NW–SE, which accommodates regional compression in the Visayan Sea Basin (Negros–Cebu–Bohol area) and the active deformation exerted along the Philippine Fault (Aurelio 2000; Yoshida et al. 2016).

Extensional and positive flower structures in a compressive environment are typical indicators of oblique compression or transpression. The extensional structures are formed due to localized extension in a transpressional fault zone (Sanderson and Marchini 1984) or through hinge-parallel extension that accommodates folding (Jamison 1991; Teyssier et al. 1998). Extension is most probably related to the pull-apart structure in Clarin and the northeast-trending linear valleys located northeast of the study area (Felix 2017). The positive flower structures, on the other hand, are subsurface features in a transpressional regime that exhumes subsurface materials as pressure ridge or pop-ups at the surface (Harding and Lowell 1979; Haberland et al. 2007). Positive flower structures are also possibly related to large-scale transpressional orogen and pop-up structures located southwest of Clarin (Felix 2017). Furthermore, the steep dip of the faults delineated in all seismic profiles are consistent with earlier findings that the North Bohol Fault has a lateral component based on focal mechanism solutions and other field evidences such as the measured pitch orientations and large-scale morphotectonic features distributed along the fault trace.

The distinct North Bohol Fault trace identified in all seismic transect sites exhibit similar strike and dip measurements suggesting that the fault is continuous from Inabanga to Clarin. Although there are gaps in between fault surface ruptures, these could be attributed to the nature of reverse faults where some segments of the fault do not reach the surface (Stein and King 1984; Stein and Yeats 1989). Faults other than those that connect with the surface are newly identified and may be part of the strike–slip fault system. They occur subparallel to the fault system either as relay or anastomosing faults in profile view defining a wider deformation zone than the rupture zone developed during the 2013 Bohol earthquake. These faults within the deformation zone identified in the seismic profiles likely to converge into a single main

strand at greater depths (e.g., Boyer and Elliott 1982; Sylvester 1988) as expressed in the regional seismic profile (Aurelio et al. 2013; Rimando 2015).

The interpretation of the Inabanga–Clarin portion of the North Bohol Fault using the seismic data has several implications for seismic hazard research: (1) subtle linear features interpreted in the LiDAR-derived images are the geomorphic expression of the identified underlying faults. This implies that the North Bohol Fault was mapped thoroughly using LiDAR by Felix (2017) and could be used for avoidance of surface rupture zones. However, other buried faults seen from seismic profiles are not expressed on the surface; (2) the accommodation of slip through folding is responsible for the wide interval of surface rupturing earthquakes along the NBF. For example, there could be more than two earthquake events that may have occurred within the wide deformation zone of the NBF (Rimando 2015). The folds that are associated with the NBF, therefore, should also be considered as sites of critical earthquake risk (Stein and King 1984); and (3) the seismic profiles can be used to better understand the geometry and kinematics of fault movement of the NBF.

Conclusions

The North Bohol Fault is a prime example that a large convergent structure may be subjected to oblique deformation near the surface rather than solely as compression. The oblique deformation near the surface is expressed as morphotectonic features as well as shallow subsurface structures, which can be seen through satellite imageries and shallow seismic reflection profiles, respectively. In the NBF, three high-resolution seismic reflection images were collected in Inabanga and Clarin to analyze its shallow subsurface geometry. The main findings of this study are the clear evidence of subsurface compressional structures such as reverse faults and contractional relays. The study also identified normal faults, flower structures, and steeply dipping faults that further support the inference that the NBF is in a transpressional regime (Felix 2017). The study also determined the orientation of NW–SE trending compression, which suggests the direction of the maximum horizontal stress accommodating the slip along the Philippine Fault. In addition, the study revealed that the topographic flexures are the surface expression of buried faults related to the recently discovered NBF. Correspondingly, these topographic flexures which previously could not be determined as rupture zones due to unclear manifestation of surface rupture is now identified as part of the NBF increasing the ground rupture length from 6 km (PHIVOLCS 2013) to 13 km length. It also validates newly identified lineaments because of the identification of faults in

Gacusan and Lagmay *Geosci. Lett.* (2019) 6:9

Page 9 of 10

the seismic profiles. Thus, the ground rupture zone is extended in terms of its width. Lastly, fault-related folds indicate repeated earthquake events that may have contributed to the development of present-day morphology. Therefore, the folds are considered as sites of earthquake risk. This study demonstrates that the combination of high-resolution seismic reflection and topographic data can be used to describe the characteristics of earthquake faults. All these findings are critical for seismic risk assessment necessary for prevention and mitigation of earthquake hazards. Without it, poor preparedness planning may result in more losses and damages in the event of future earthquake.

Authors' contributions
RCTG and AMFAL decided on the study and methodology. RCTG carried out the data acquisition, processing, and manuscript writing with inputs from AMFAL. Both authors interpreted and discussed the results obtained and finalized the manuscript. Both authors read and approved the final manuscript.

Availability of data and materials
All data generated for this study are included in this published article.

Competing interests
The authors declare that they have no competing interests.

Author details
[1] National Institute of Geological Sciences, University of the Philippines, Quezon City, Philippines. [2] UP NOAH Center, University of the Philippines, Quezon City, Philippines.

References
Aurelio MA (2000) Shear partitioning in the Philippines: constraints from Philippine fault and global positioning system data. Island Arc 9:584–597. https://doi.org/10.1111/j.1440-1738.2000.00304.x

Aurelio MA, Rimando JM, Taguibao KJL, Dianala JDB, Berador AE (2013) Seismotectonics of the magnitude 7.2 Bohol earthquake of 15 october 2013 from onshore, earthquake and offshore data: a key to discovering other buried active thrust faults. In: The 26th annual geological convention: invest in geology, invest in the future, Makati, PH. Geological Society of the Philippines

Baker GS (1999) Processing near-surface seismic-reflection data: a primer. Society of Exploration Geophysicist, Tulsa. https://doi.org/10.1190/1.9781560802020

Baker GS, Steeples DW, Drake M (1998) Muting the noise cone in near-surface reflection data: an example from southeastern Kansas. Geophysics 63:1332–1338. https://doi.org/10.1190/1.1444434

Ben-Zion Y, Sammis C (2003) Characterization of fault zones. Pure Appl Geophys 160(3):677–715. https://doi.org/10.1007/PL00012554

BMG (1987) Geologic maps of Bohol Island. Technical report, Bureau of Mines and Geosciences (BMG), Department of Environment, Energy, and Natural Resources

Boyer SE, Elliott D (1982) Thrust systems. Am Assoc Pet Geol Bull 66(9):1196–1230

Bruno PPG, Pazzaglia FJ, Picotti V (2011) Evidence for active folding and faulting at the Northern Apennines mountain front near Bologna italy from high resolution seismic reflection profiling. Geophys Res Lett. https://doi.org/10.1029/2011GL047828

Corby GW, Kleinpell RM, Popenoe WP, Merchant R, William H, Teves J, Grey R, Daleon B, Mamaclay F, Villongco A, Herrera M, Guillen J, Hollister JS, Johnson HN, Billings MH, Fryxell EM, Taylor EF, Nelson CN, Birch DC, Reed RW, Marquez R (1951) Geology and oil possibilities of the Philippines. Technical Bulletin 21. Bureau of Mines, DANR, p 365

Dolan JF, Pratt TL (1997) High-resolution seismic reflection profiling of the Santa Monica fault zone, West Los Angeles, California. Geophys Res Lett 24(16):2051–2054. https://doi.org/10.1029/97GL01940

Felix RP (2017) Detailed mapping of the north Bohol fault in Bohol, Philippines using high-resolution topographic models and field analysis. Master's thesis, University of the Philippines

Goswami CC, Mukhopadhyay D, Poddar BC (2013) Geomorphology in relation to tectonics: a case study from the eastern Himalayan foothills of West Bengal, India. Quat Int 298:80–92. https://doi.org/10.1016/j.quaint.2012.12.020

Haberland C, Maercklin N, Kesten D, Ryberg T, Janssen C, Agnon A, Weber M, Schulze A, Qabbani I, El-Kelani R (2007) Shallow architecture of the Wadi Araba fault (Dead Sea transform) from high-resolution seismic investigations. Tectonophysics 432:37–50. https://doi.org/10.1016/j.tecto.2006.12.006

Harding TP, Lowell JD (1979) Structural styles, their plate-tectonic habitats, and hydrocarbon traps in petroleum provinces. Am Assoc Petrol Geol Bull 63(7):1016–1058

Jamison WR (1991) Kinematics of compressional fold development in convergent wrench terranes. Tectonophysics 190:209–232. https://doi.org/10.1016/0040-1951(91)90431-Q

Lagmay AMF, Eco RN (2014) Brief communication: on the source characteristics and impacts of the magnitude 7.2 Bohol earthquake, Philippines. Nat Hazards Earth Syst Sci Discuss 2:2103–2115. https://doi.org/10.5194/nhess-14-2795-2014

MGB (2014) Ground penetrating radar (GPR) investigations and geohazards assessment in the municipality of Inabanga/Clarin, province of Bohol. Technical report, Mines and Geosciences Bureau

Mousa WA, Al-Shuhail AA (2011) Processing of seismic reflection data using MATLAB™. Synth Lect Signal Process 5(1):1–97. https://doi.org/10.2200/S00384ED1V01Y201109SPR010

Mula EY, Maac YO (1995) Biostratigraphic studies in Bohol Island: report of research and development cooperation. itit project no. 8313 (research for enhancement of reference sections of sedimentary basins in the Philippines. Technical report, Geological Survey of Japan

NDRRMC (2013) Sitrep 35 re effects of magnitude 7.2 Sagbayan, Bohol earthquake. Techreport, National Disaster Risk Reduction and Management Council (NDRRMC), Quezon City, Philippines

Nicol A, Gillespie PA, Childs C, Walsh JJ (2002) Relay zones between mesoscopic thrust faults in layered sedimentary sequences. J Struct Geol 24:709–727. https://doi.org/10.1016/S0191-8141(01)00113-4

Peña RE (2008) Lexicon of Philippine Stratigraphy. Geological Society of the Philippines, Mandaluyong City, Philippines

PHIVOLCS (2013) The 15 october 2013 m7.2 Bohol earthquake. Technical report, Philippine Institute of Volcanology and Seismology

Pratt TL, Dolan JF, Odum JK, Stephenson WJ, Williams RA, Templeton ME (1998) Multiscale seismic imaging of active fault zones for hazard assessment: a case study of the Santa Monica fault zone, Los Angeles, California. Geophysics 63(2):479–489. https://doi.org/10.1190/1.1444349

Pratt TL, Shaw JH, Dolan JF, Christofferson SA, Williams RA, Odum JK, Plesch A (2002) Shallow seismic imaging of folds above Puente Hills blind-thrust

fault, Los Angeles, California. Geophys Res Lett 29:18. https://doi.org/10.1029/2001GL014313

Rimando JM (2015) Ground deformation associated with the october 15, 2013 magnitude (m_w) 7.2 Bohol earthquake, Bohol Island, Philippines. Master's thesis, University of the Philippines

Sanderson DJ, Marchini WRD (1984) Transpression. J Struct Geol 6(5):449–458. https://doi.org/10.1016/0191-8141(84)90058-0

Sandmeier K-J (2016) Reflexw v8.0: Windows XP/7/8/10-program for processing of seismic, acoustic or electromagnetic reflection, refraction and transmission data. http://www.sandmeier-geo.de/Download/reflexw_manual_a4.pdf. Accessed 15 Sept 2016

Stein RS, King GCP (1984) Seismic potential revealed by surface folding: 1983 Coalinga, California, earthquake. Science 224:869–873. https://doi.org/10.1126/science.224.4651.869

Stein RS, Yeats RS (1989) Hidden earthquakes. Sci Am 260(6):48–57. https://doi.org/10.1038/scientificamerican0689-48

Suppe J (1983) Geometry and kinematics of fault-bend folding. Am J Sci 283:684–721. https://doi.org/10.2475/ajs.283.7.684

Suppe J, Medwedeff DA (1990) Geometry and kinematics of fault-propagation folding. Eclogae Geol Helv 83(3):4

Sylvester AG (1988) Strike-slip faults. Geol Soc Am Bull 100:1666–1703. https://doi.org/10.1130/0016-7606(1988)100<1666:SSF>2.3.CO;2

Teyssier C, Tikoff B (1998) Strikewd–slip partitioned transpression of the San Andreas fault system: a lithospheric-scale approach. In: Holdsworth RE, Strachan RA, Dewey JF (eds) Continental Transpressional and Transtensional Tectonics. Special Publications, vol. 135. The Geological Society, London, pp. 143–158

Wells DL, Coppersmith KJ (1994) New empirical relationships among magnitude, rupture length, rupture width, rupture area, and surface displacement. Bull Seismol Soc Am 84:974–1002

Yilmaz O (1987) Investigations in geophysics no. 2: seismic data processing. Society of Exploration Geophysicist, Tulsa. https://doi.org/10.1190/1.9781560801580

Yoshida K, Pulido N, Fukuyama E (2016) Unusual stress rotations within the Philippines possibly caused by slip heterogenity along the Philippine fault. J Geophys Res 121:2020–2036. https://doi.org/10.1002/2015JB012275

Publisher's Note